Int. J. Electrochem. Sci., 7 **(2012)** 671 - 685

International Journal of
ELECTROCHEMICAL
SCIENCE
www.electrochemsci.org

New composite Anodes for oxygen Evolution during seawater Electrolysis

A. A. El-Moneim[1,2,*] *and M. B. Mohamed*[1]

[1] Egypt-Japan University of Science and Technology, Materials Science and Engineering Department, New Borg El-Arab, Alexandria 21934, Egypt.
[2] Physical chemistry department, National Research Centre, Giza, Egypt.
[*]E-mail: ahmed.abdelmoneim@ejust.edu.eg

Received: 14 October 2011 / *Accepted:* 30 November 2011 / *Published:* 1 January 2012

For $Mn_{0.92}Mo_{0.07}Sn_{0.01}O_{2.07}/Sn_{1-x-y}Ir_xSb_yO_{2+0.5y}$/Ti anodes, with x and y in the range of 0.135-1.0 and 0.05-0.16, respectively, the replacement of the IrO_2 in the intermediate layer with $Sn_{1-x-y}Ir_xSb_yO_{2+0.5y}$ was effective in elongating the life of the anodes during oxygen evolution without forming chlorine in seawater electrolysis. The longest life was realized by the formation of uniform single phase $Sn_{1-x-y}Ir_xSb_yO_{2+0.5y}$ intermediate layer with compact structure. The life of the anodes using triple oxide intermediate layer increased with the increase in the Ir content due to an increase in both electrical conductivity and grain size of the oxide structure.

Keywords: anode, durability, oxidation of titanium, activity, electrical conductivity of oxide.

1. INTRODUCTION

In seawater electrolysis for hydrogen production the anodic reaction should not form chlorine but oxygen. The present authors and others use oxide anodes composed of three layers; outer electrocatalyst oxide, intermediate conductive oxide layer and inner titanium substrate [1-10]. Different outer electrocatalyst layers with initial 100% oxygen evolution efficiency at electrolysis current density of 1000 Am^{-2} in 0.5 M NaCl solution were developed [1-10]. Those were anodically deposited γ-MnO_2 type multiple oxides of MnW [1,2], MnMo [3,4], MnMoW [1,5,6], MnMoFe [7,8] and MnMoSn [9,10]. The MnMoX (X = Fe^{3+}, W^{6+}, Sn^{4+})-triple oxide anodes have shown better performance over MnY(Y = Mo^{6+}, W^{6+})-double oxide anodes. The Sn^{4+} cation was the best compared with Fe^{3+} and W^{6+} cations during long term electrolysis of the triple oxides.

Because of the aggressive conditions of the electrolysis process, that is anodic polarization at high current density in NaCl solution, titanium is generally used as a conductive substrate. However, anodic polarization of titanium immediately results in the formation of insulating titanium dioxide, TiO_2. In order to avoid the TiO_2 formation, the titanium substrate is usually covered by conductive iridium dioxide, IrO_2. The IrO_2, has the same rutile structure as TiO_2, and is formed by calcinations of chloroiridic acid butanol solution coated on the titanium substrate [5-10]. In fact, the IrO_2-covered titanium can generally be used as an oxygen evolution anode in aqueous solutions without chloride ions. However, if chloride ions are contained in the electrolyte, chlorine evolution occurs preferentially on the IrO_2-covered titanium. Hence, there is still a need to prepare durable γ-MnO_2-type electrocatalysts on a low cost, stable and conductive intermediate layer for oxygen evolution in seawater electrolysis.

Degradation of γ-MnO_2-type electrocatalysts/IrO_2/Ti anode occurs due to partial detachment of the outer electrocatalyst layer by its internal mechanical stresses and/or growth of interlayer insulating TiO_2 at the interface of IrO_2/Ti electrode [5,6]. Therefore, the alternative oxides to IrO_2 have low cost, sufficient protectiveness and conductivity at high potentials for anodic polarization and the same rutile structure as TiO_2 are required. Among RuSn- [11-14], RuTiSn- [15,16], IrTi- [17,18], IrTa- [19,20], IrSn- [21,22], RuSbSn- [23] and SnIrSb-oxides examined so far, SnIrSb-oxide showed the excellent protection to Ti substrate against oxidation by anodic polarization. It was found that the dispersion of Ir^{4+} ions in Sb_2O_5–SnO_2 oxide formed from a coating solution of 10 mol % of iridium showed an excellent performance of a service life of 1600 h by electrolysis in 3 M H_2SO_4 solution at a current density of 10000 Am^{-2} at 35°C compared with 355 h for IrO_2 electrode [24]. However, understanding how the dispersion of Ir^{4+} ions in SnO_2-Sb_2O_5 oxide, is adopted for improving the protectiveness to Ti substrate still needs further clarifications.

The present work is undertaken to examine the possibility to use SnIrSb-oxide intermediate layer for improving the durability of γ-MnO_2-type MnMoSn-oxide electrocatalyst for the oxygen evolution efficiency during electrolysis of 0.5 M NaCl solution at the current density of 1000 Am^{-2}. Particular attention is given to understand the performance, electrochemical and structure characteristics of SnIrSb-oxide coated Ti substrate.

2. EXPERIMENTAL

A punched titanium substrate mesh of 100 x 50 x 1 mm was polished in 0.5 M HF solution for 5 min for removal of air-formed oxide. In order to ensure a better adherence of the outer and intermediate layers to the inner titanium substrate, surface-roughening of the titanium substrate was carried out by etching in 11.5 M H_2SO_4 solution at 80^oC until hydrogen evolution was ceased. Pre-treated Ti substrate was coated with SnIrSb-oxide active layers by a thermal decomposition of 0.5M $SnCl_4$, $5H_2O$, 0.5M $SbCl_5.5H_2O$ and 0.5M H_4IrCl_6/butanol in precursor mixtures. The SnIrSb-oxides were produced by combining various proportions of Ir^{4+} species with Sn^{4+} and Sb^{5+} in molar ratio of 90:10. The applied coating was dried at 90°C in air for 10 min, and then fired at 550°C for 5 min. The operation of coating, drying and firing was repeated several times to achieve the desired loading of

oxide and thickness. The electrode was finally annealed at 550°C for 1 h. The loading of the oxides estimated by the weight increase of the sample after the finish of preparation was 0.75~1.07 gm^{-2}. The prepared sample was then cut into pieces of 15.3 x15.3 x1.5 mm for surface and electrochemical characterizations, as well as stability test. IrO_2/Ti electrode was prepared employing the same procedure described above.

The outer MnMoSn-oxide electrocatalyst layer was anodically deposited on the clean and activated SnIrSb-oxide/Ti and IrO_2/Ti electrodes in the mixture of aqueous solution of 0.2 M $MnSO_4.5H_2O$-0.003 M $Na_2MoO_4.2H_2O$-0.006 M $SnCl_4.5H_2O$ of pH –0.1 at 600 $Am^{-2}$and 90^oC for 60 minutes. The thickness of the outer electrocatalyst layer was estimated from the mass difference before and after deposition and densities of MnO_2, MoO_3 and SnO_2 [9,10].

The oxygen evolution efficiency of MnMoSn-oxide/SnIrSb-oxide/Ti anodes was measured by electrolysis at a constant current density of 1000 Am^{-2} in 0.5 M NaCl solution of pH 8.7 until the amount of charges of 300 coulombs was passed. The amount of oxygen evolved was determined as the difference between the total charge passed and the charge for chlorine formation during electrolysis as described elsewhere [26, 27]. The activity of the anodes for oxygen evolution was examined by IR corrected galvanostatic polarization measurements in 0.5 M NaCl solution of pH 8.7.

To understand the effect of the intermediate SnIrSb-oxide layers on the anode durability during seawater electrolysis, the following tests were carried out on SnIrSb-oxide/Ti electrodes; i. Accelerated life test in 3 M H_2SO_4 solution at a current of 10000 Am^{-2} and 40^oC to evaluate the stability of these electrodes [25], ii. Cyclic voltammetry using potential scan rates of ν = 2 to 150 mVs^{-1} to furnish information surface electrochemistry, capacity and roughness factor, iii. IR corrected polarization measurements in 0.5 M H_2SO_4 solution to clarify the activity of the electrodes for oxygen evolution reaction.

All electrochemical measurements were performed using an electrochemical cell with two compartments and three electrodes with platinum foil as a counter electrode and Ag/AgCl/ KCl (sat.) as a reference electrode.

The composition and morphology of outer and intermediate coatings were analyzed by electron probe micro analyzer. The crystal structure of the coatings was identified by X-ray diffraction by α-2θ mode at a glancing angle α of 5^o using Rigaku RINT X-ray diffractometer with Cu Kα radiation.

3. RESULTS

3.1. Composition of outer and intermediate layers in MnMoSn-oxide/SnIrSb-oxide/Ti anodes.

The oxidation states of the cations in the outer MnMoSn-oxide electrocatalyst layer were identified as Mn^{4+}, Mo^{6+} and Sn^{4+} [9,10] and hence, the electrocatalyst will be denoted hereafter by the following formula $Mn_{1-z-s}Mo_zSn_sO_{2+z}$. Where, z and s are the determined cationic fractions of molybdenum and tin in oxide coatings, respectively. The average values of z and s are 0.07 and 0.01, respectively. Meanwhile, the oxidation states of the cations in the intermediate SnIrSb-oxide layers were identified as Sn^{4+}, Sb^{5+} and Ir^{4+} [28] and hence, all the intermediate SnIrSb-oxide layers will be

denoted hereafter by the following formula $Sn_{1-x-y}Ir_xSb_yO_{2+0.5y}$. Where, x and y are the determined cationic fractions of Ir and Sb species in the oxide coatings, respectively. The values of x and y are in the range of 0.13-1.0 and 0.05-0.16, respectively. The antimony/tin ratio in all $Sn_{1-x-y}Ir_xSb_yO_{2+0.5y}$ coatings is in the range of 0.125-0.17.

3.2. Performance and characteristics of $Mn_{0.92}Mo_{0.07}Sn_{0.01}O_{2.07}/Sn_{1-x-y}Ir_xSb_yO_{2+0.5y}$/Ti anodes during seawater electrolysis.

Figure 1 shows the change in the oxygen evolution efficiency for $Mn_{0.92}Mo_{0.07}Sn_{0.01}O_{2.07}/Sn_{1-x-y}Ir_xSb_yO_{2+0.5y}$/Ti anodes with Ir content, x, in the range of 0.13-1.0, as a function of time of electrolysis in 0.5 M NaCl solution at 1000 Am^{-2}.

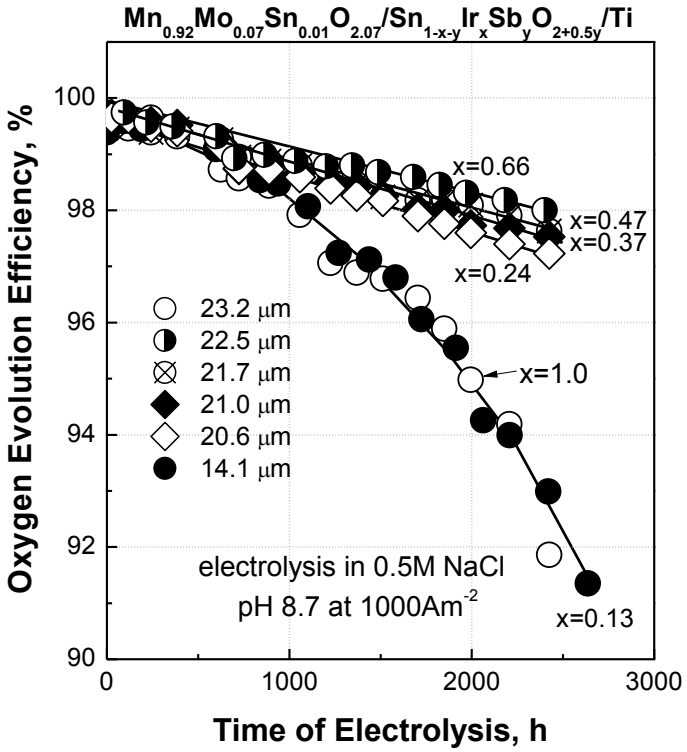

Figure 1. Change in oxygen evolution efficiency for $Mn_{0.92}Mo_{0.07}Sn_{0.01}O_{2.07}/Sn_{1-x-y}Ir_xSb_yO_{2+0.5y}$/Ti anodes as a function of time of electrolysis in 0.5 M NaCl solution of pH 8.7 at 1000 Am^{-2}. The thicknesses of outer electrocatalyst layer are written in the figure.

The thicknesses of the deposited outer electrocatalyst layer are written in the figure. As shown, all anodes show 100% initial oxygen evolution efficiency. Afterwards, the oxygen evolution efficiency decreases with electrolysis. Expect for $Mn_{0.92}Mo_{0.07}Sn_{0.01}O_{2.07}/IrO_2$/Ti anode, x = 1.0, the oxygen evolution efficiency tends to increase with the increase in the Ir content. On the other hand, the $Mn_{0.92}Mo_{0.07}Sn_{0.01}O_{2.07}/Sn_{1-x-y}Ir_xSb_yO_{2+0.5}$/Ti anodes with Ir content in the range of 0.24-0.66 show oxygen evolution efficiency higher than 97.5% for more than 2400 h of electrolysis. While, $Mn_{0.92}Mo_{0.07}Sn_{0.01}O_{2.07}/ Sn_{1-x-y}Ir_xSb_yO_{2+0.5}$/Ti anodes with Ir content of 0.13 and 1.0 show 91.2 and

92.0 % oxygen evolution efficiency for more than 2400 h, respectively. Thus, the performance of the anodes with the intermediate $Sn_{1-x-y}Ir_xSb_yO_{2+0.5}$ triple oxide layers with sufficient Ir content is superior to that of the anode with the IrO_2 intermediate layer.

The effect of the composition of the intermediate layer on the anode stability was examined by measuring the loss in the anode weight during intervals of electrolysis using weight loss measurement technique. The results revealed that the anodes with triple oxide intermediate layers with Ir content in the range of 0.24-0.66 suffer from no lose in their weight during electrolysis. While, the anode with IrO_2 intermediate layer lost about 5.5% of its weight after 2400 h of electrolysis.

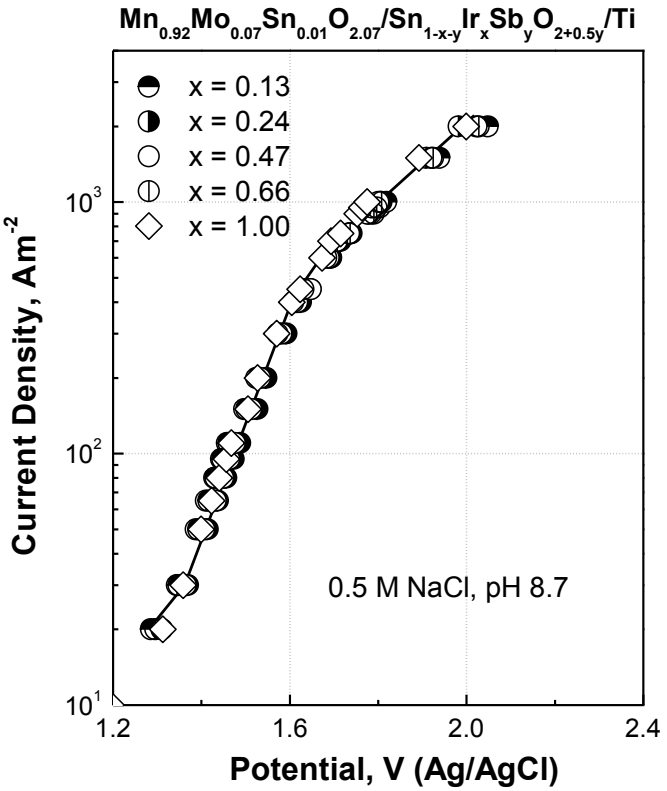

Figure 2. IR corrected galvanostatic polarization curves of $Mn_{0.92}Mo_{0.07}Sn_{0.01}O_{2.07}/Sn_{1-x-y}Ir_xSb_yO_{2+0.5y}$/Ti anodes in 0.5 M NaCl solution of pH 8.7.

Figure 2 shows IR-corrected galvanostatic polarization curves of as prepared $Mn_{0.92}Mo_{0.07}Sn_{0.01}O_{2.07}/Sn_{1-x-y}Ir_xSb_yO_{2+0.5y}$/Ti anodes measured in 0.5 M NaCl solution at pH 8.7. As seen in Fig. 2, the initial activity of the anodes for oxygen evolution reaction is generally independent of the composition of the intermediate layer. However, the recorded polarization potentials of the $Mn_{0.92}Mo_{0.07}Sn_{0.01}O_{2.07}/Sn_{1-x-y}Ir_xSb_yO_{2+0.5}$/Ti anodes with x = 0.24, 0.66 and 1.0 after 2400 h of electrolysis in 0.5 M NaCl solution at $1000Am^{-2}$ are 2.01, 1.92 and 2.35 V(Ag/AgCl), respectively. This indicates that the composition of the intermediate layer plays a vital role in controlling the activity of the anodes during electrolysis.

In the X-ray diffraction patterns of as the prepared anodes, only γ-MnO_2 type oxide is identified and no other diffraction lines of separate oxides of molybdenum and tin were observed, as

seen in Fig. 3. Consequently, the deposits were composed of a single phase of $Mn_{1-z-s}Mo_zSn_sO_{2+z}$ triple oxide of the γ-MnO_2 type structure.

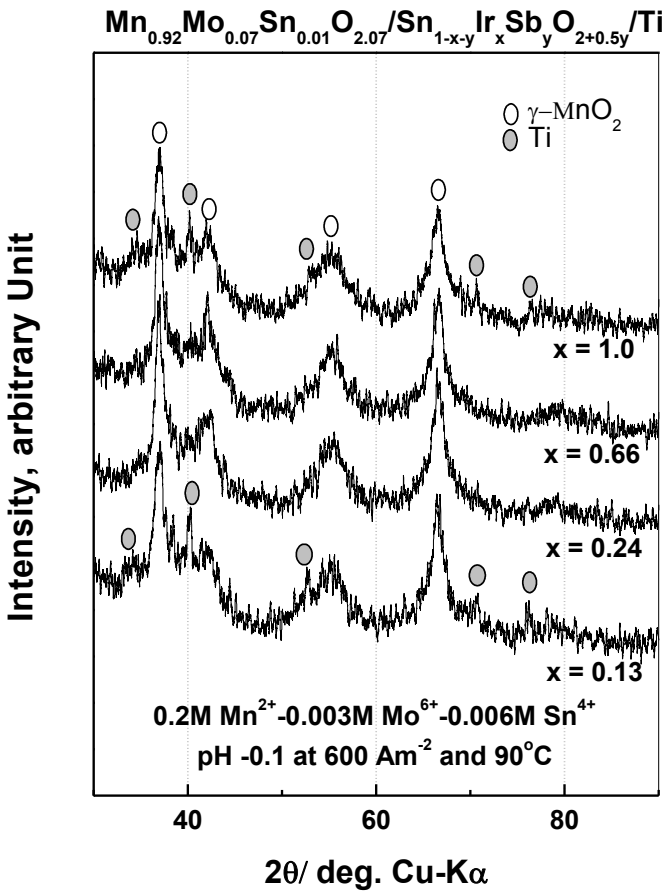

Figure 3. XRD patterns of $Mn_{0.92}Mo_{0.07}Sn_{0.01}O_{2.07}/Sn_{1-x-y}Ir_xSb_yO_{2+0.5}$/Ti anodes with Ir content, x, in the range of 0.13-1.0.

On the other hand, the fainted reflection lines of Ti substrate are only detected for the electrode deposited on the intermediate layers with Ir content, x, of 0.13 and 1.0. This confirms the insufficient coverage of the outer electrodeposited layer to the intermediate layer, which actively evolves chlorine, and correlated with its low durability for oxygen evolution during seawater electrolysis as presented in Fig. 1. Considering the fact that the thickness of the electrocatalyst film deposited on IrO_2/Ti electrode, x = 1.0, is the largest among all the examined outer deposited films (Fig.1), it can be assumed that the insufficient coverage of the outer electrocatalyst layer to the intermediate IrO_2 layer coated titanium substrate seems to be mainly due to unevenness of the intermediate IrO_2 film, as confirmed later in Fig. 5.

To understand the beneficial effect of the intermediate $Sn_{1-x-y}Ir_xSb_yO_{2+0.5y}$ triple oxide layer in enhancing the anode durability during seawater electrolysis, accelerated service life test, structure and electrochemical characterizations measurements were carried out on $Sn_{1-x-y}Ir_xSb_yO_{2+0.5y}$/Ti electrodes.

3.3. Performance and characteristics of $Sn_{1-x-y}Ir_xSb_yO_{2+0.5y}$/Ti electrodes before and during service life test.

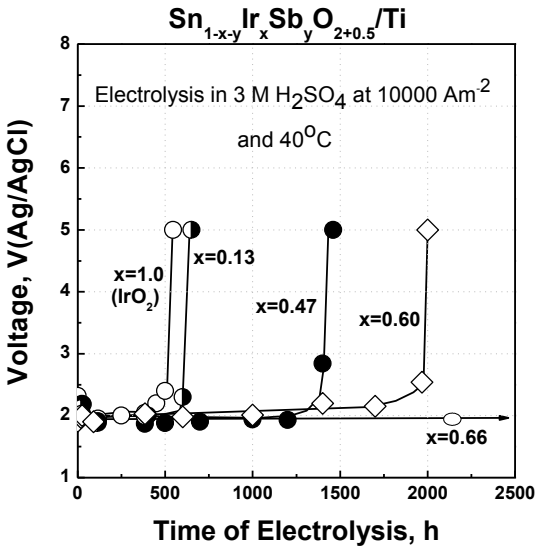

Figure 4.Change in potentials of $Sn_{1-x-y}Ir_xSb_yO_{2+0.5}$/Ti electrodes with Ir content, x, in the range of 0.13-1.0 during electrolysis of 3 M H_2SO_4 at 10000 Am^{-2} and 40^oC.

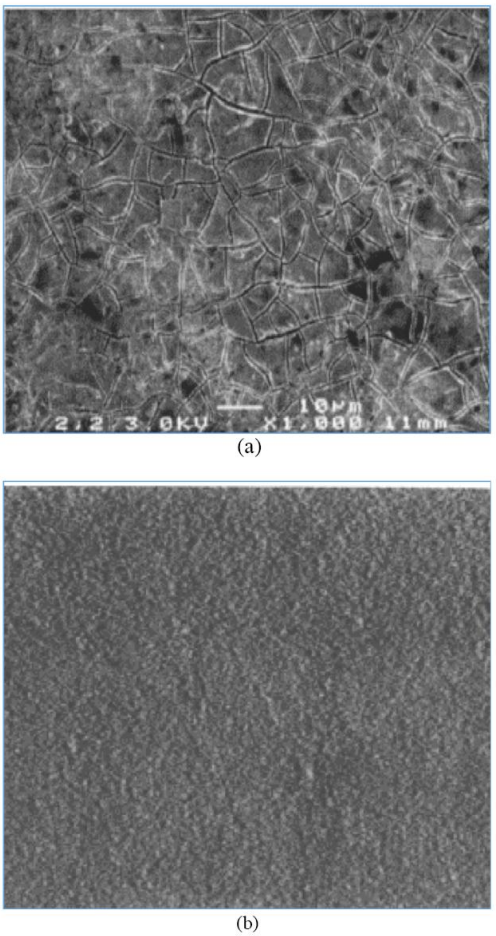

Figure 5. Scanning electron micrographs of anodes with the electrocatalysts of IrO_2 (a) and $Sn_{0.40}Ir_{0.47}Sb_{0.13}O_{2.06}$ (b).

Figure 4 shows the accelerated service life test of $Sn_{1-x-y}Ir_xSb_yO_{2+0.5y}$/Ti electrodes in 3 M H_2SO_4 solution at 40°C and 10000 Am^{-2}. Test end upon 1 volt increase in the continuously recorded cell potential is reached. As shown, all $Sn_{1-x-y}Ir_xSb_yO_{2+0.5y}$/Ti electrodes show longer life than IrO_2/Ti electrode. The life of the $Sn_{1-x-y}Ir_xSb_yO_{2+0.5y}$/Ti electrodes increases with the increase in Ir content of the coating, where no degradation was found for the triple oxide electrode with Ir content, x, of 0.66 even after electrolysis for more than 2200 h. Hence, the $Sn_{1-x-y}Ir_xSb_yO_{2+0.5y}$/Ti electrodes beneficially save IrO_2 loading and have better stability than IrO_2/Ti electrode.

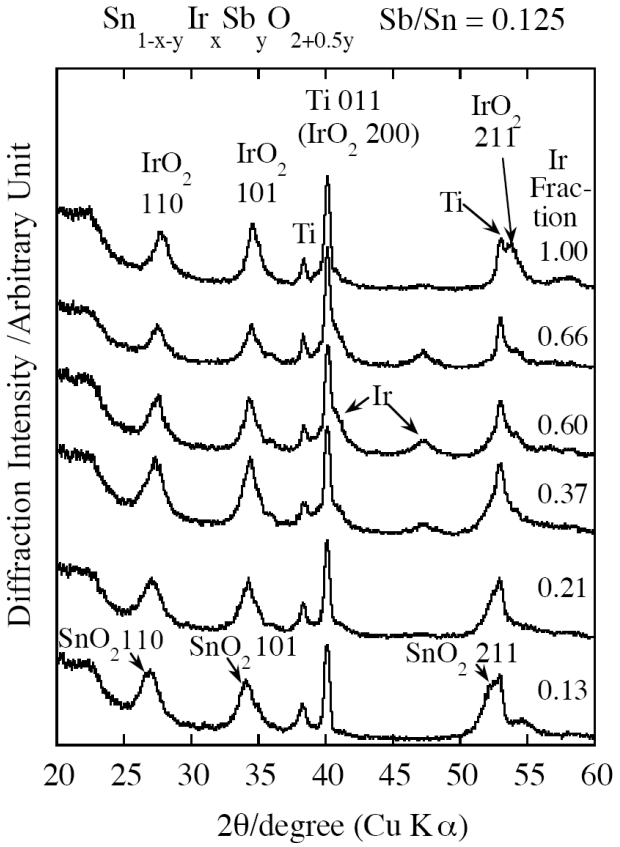

Figure 6. XRD patterns of $Sn_{1-x-y}Ir_xSb_yO_{2+0.5}$/Ti electrodes with Ir content, x, in the range of 0.13-1.0.

Figure 5 (a) and (b) shows SEM images of IrO_2 and $Sn_{0.40}Ir_{0.47}Sb_{0.13}O_{2.06}$ oxides coated-Ti substrate, respectively. The morphology of IrO_2 coating, Fig. 5(a), is characterized by uneven structure with a high density of grooves, which can provide easy and short paths for the inward diffusion of oxygen to the titanium surface. In contrast to the IrO_2 coating, $Sn_{0.40}Ir_{0.47}Sb_{0.13}O_{2.06}$ coating is characterized by an even surface without apparent grooves as in Fig. 5(b).

Figure 6 shows X-ray diffraction patterns of as prepared $Sn_{1-x-y}Ir_xSb_yO_{2+0.5y}$/Ti electrodes. Substances identified by all diffraction patterns are only rutile type body-centered tetragonal oxide and titanium of the substrate in addition to metallic iridium. IrO_2 and SnO_2 have the same rutile-type tetragonal structure, and the lattice constants, a^0 and c^0, of SnO_2 are larger than those of IrO_2 [23,24]. In Fig. 6, the diffraction angles of tetragonal oxides decrease with decreasing iridium content, indicating an increase in lattice constants with an increase in tin content. This fact shows that the tin

content in the tetragonal oxide increases with a decrease in the content of iridium. Thus, the oxide consists of a solid solution of a single phase triple oxide.

The mean grain size of $Sn_{1-x-y}Ir_xSb_yO_{2+0.5y}$ triple oxides was estimated from the full width at half maximum of 110 reflection of the $Sn_{1-x-y}Ir_xSb_yO_{2+0.5y}$ oxide coatings using Sherrer's equation [28] and presented in Fig. 7 as a function of iridium content of the coatings. As seen, the grain size increases almost linearly with an increase in Ir content of the oxides. In principle, the distance for the inward diffusion of passivating oxygen from the outer surface of the electrocatalyst to the electrocatalyst/substrate interface is known to increase with the grain coarsening of the oxide microstructure.

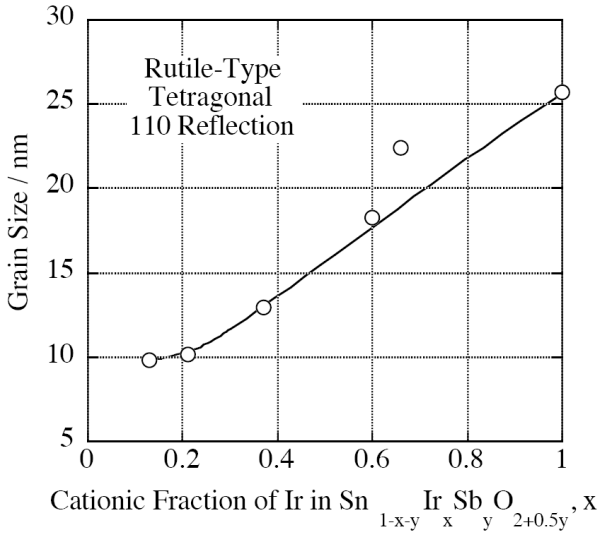

Figure 7. Grain size estimated from the 110 reflection of the rutile-type tetragonal oxides in Fig. 6.

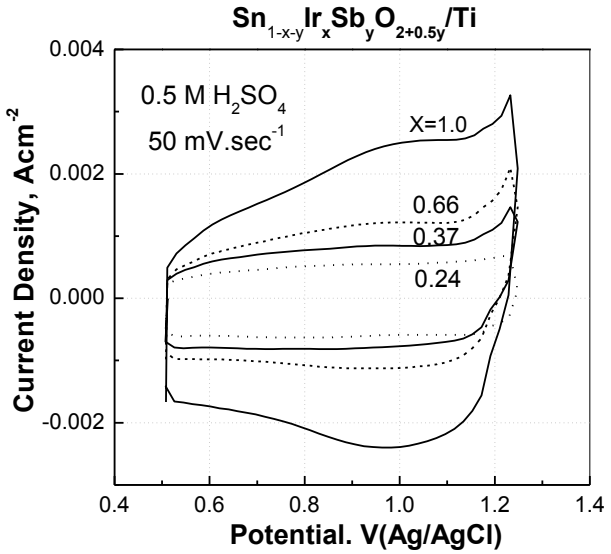

Figure 8. Cyclic voltammetry profiles of as prepared $Sn_{1-x-y}Ir_xSb_yO_{2+0.5}$/Ti electrodes with Ir content, x, in the range of 0.13-1.0 in 0.5 M H_2SO_4 solution.

In-situ voltammetric characterization usually furnishes important information about the surface electrochemistry, capacity and roughness factor [19,20], which are important probes in assessing the overall performance of the electrocatalyts.

Figure 8 shows typical voltammetric profiles of as prepared $Sn_{1-x-y}Ir_xSb_yO_{2+0.5y}$/Ti electrodes measured in 0.5 M H_2SO_4 solution. As shown, all electrodes exhibit a pseudocapactive behavior and the capacitive current gradually increases with the increase in Ir content. This fact indicates that the surface electrochemistry of $Sn_{1-x-y}Ir_xSb_yO_{2+0.5y}$ electrocatalysts is classically controlled by Ir content.

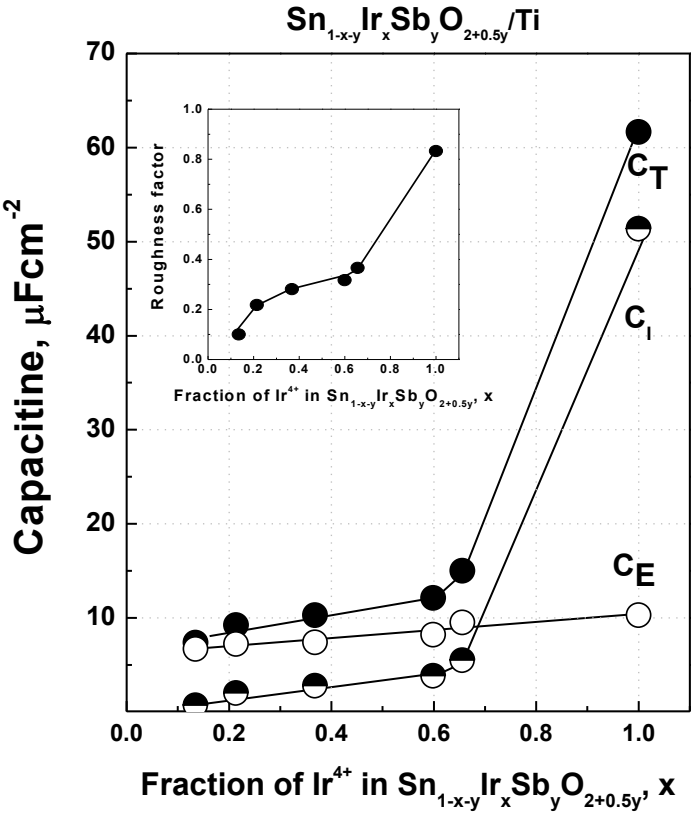

Figure 9. Variation of C_T, C_E and C_I, and φ (see the inset) surface parameters of $Sn_{1-x-y}Ir_xSb_yO_{2+0.5}$/Ti electrodes with Ir content, x.

Figure 9 summarizes the variation of the total (C_T), external (C_E) and internal (C_I) capacities surface parameters of $Sn_{1-x-y}Ir_xSb_yO_{2+0.5y}$ /Ti electrodes with the Ir content. The variation in roughness factor (φ), $\varphi=C_I/C_E$, of $Sn_{1-x-y}Ir_xSb_yO_{2+0.5y}$ /Ti electrodes with the Ir content is inserted in Fig. 9. Details about definitions and measurements of C_T, C_E, C_I and φ surface parameters are given elsewhere [20]. In Fig. 9, the values of C_T, C_I, C_E and φ for ternary oxide electrodes are about five to seven times lower than those for IrO_2/Ti electrode. This implies that the $Sn_{1-x-y}Ir_xSb_yO_{2+0.5y}$ oxide coatings tend to form more compact structure with less contribution of the inner surface compared with IrO_2 coating. For $Sn_{1-x-y}Ir_xSb_yO_{2+0.5y}$ /Ti electrodes with Ir content in the range of 0.13-0.66, the values of C_T, C_I and C_E tend to slightly increase with the increase in Ir content in the coatings. This means that the

contribution of surface area to the electrochemical activity of ternary oxide electrocatalysts with the variation in the Ir content seems to be insignificant.

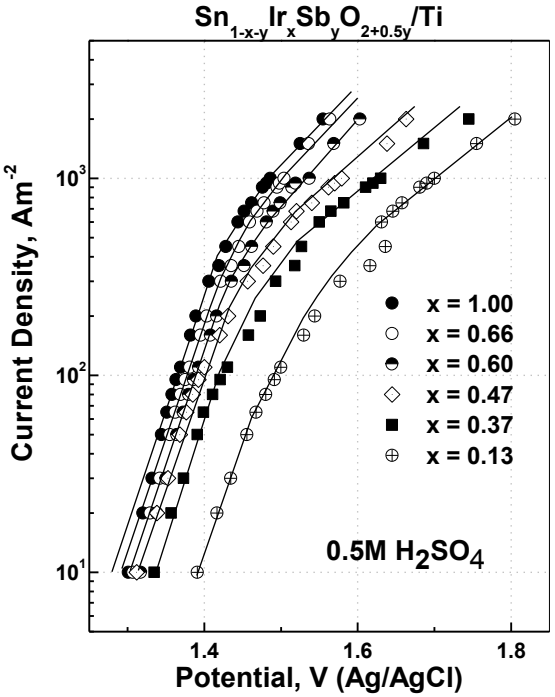

Figure 10. IR corrected galvanostatic polarization curves of $Sn_{1-x-y}Ir_xSb_yO_{2+0.5}$/Ti electrodes in 0.5 M H_2SO_4 solution.

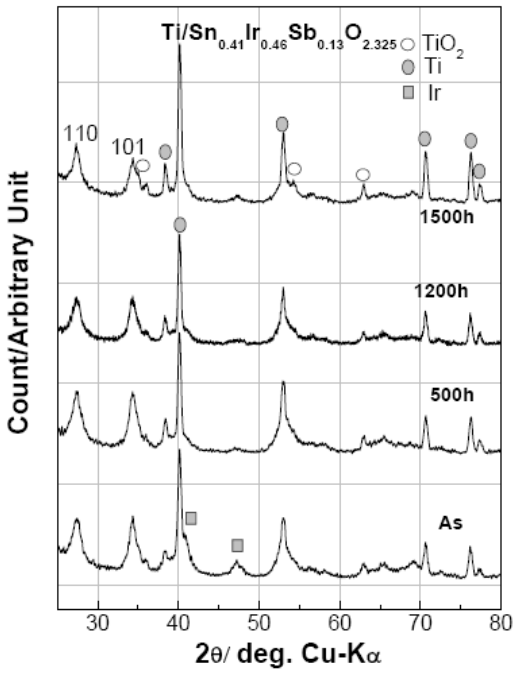

Figure 11. XRD patterns of $Sn_{0.40}Ir_{0.47}Sb_{0.13}O_{2.06}$ /Ti electrode after different intervals of electrolysis in 3 M H_2SO_4 solution at 10000 Am^{-2}.

Figure 10 presents IR corrected galvanostatic polarization curves for as prepared $Sn_{1-x-y}Ir_xSb_yO_{2+0.5y}$/Ti electrodes measured in 0.5 M H_2SO_4 solution. The electrocatalytic activity of electrodes for oxygen evolution reaction increases with the increase in the Ir content. It can, therefore, be said the increase in the electro-catalytic activity for oxygen evolution reaction with the increase in Ir content in $Sn_{1-x-y}Ir_xSb_yO_{2+0.5y}$/Ti triple oxide electrodes is due to an increase in the electrical conductivity of the oxides.

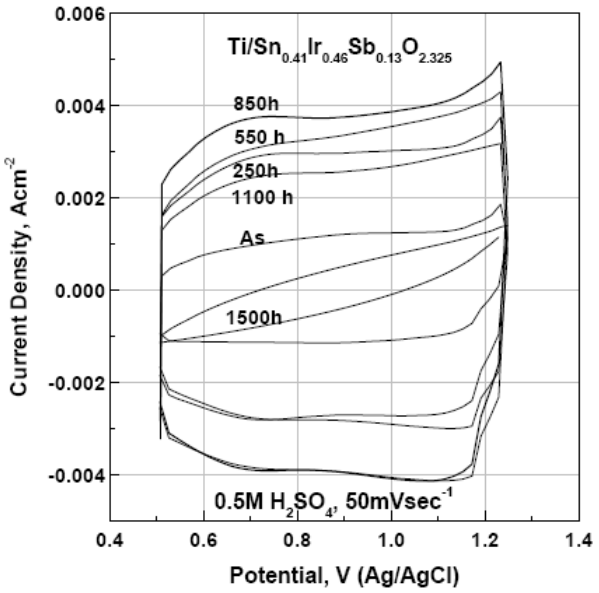

Figure 12. CV profiles of $Sn_{0.40}Ir_{0.47}Sb_{0.13}O_{2.06}$ /Ti electrode measured in 0.5 M H_2SO_4 solution after different intervals of electrolysis in 3 M H_2SO_4 solution at 10000 Am^{-2}.

Figure 11 shows XRD patterns of $Sn_{0.40}Ir_{0.47}Sb_{0.13}O_{2.06}$ /Ti electrode before and after different intervals of electrolysis in 3 M H_2SO_4 solution at 10000 Am^{-2}. As seen, the reflection peaks typical of metallic Ir are completely disappeared after 250 h of electrolysis. The reflection peaks typical of TiO_2 are recorded after deactivation at 1500 h of electrolysis. Meanwhile, the peak position and intensity of 110 and 101 planes in the rutile structure are generally unchanged with electrolysis and even after deactivation, indicating the electrochemical stability of the oxide structure.

Figure 12 shows typical voltammetric profiles of $Sn_{0.40}Ir_{0.47}Sb_{0.13}O_{2.06}$ /Ti electrode in 0.5 M H_2SO_4 solution during intervals of electrolysis in 3 M H_2SO_4 solution at 10000 Am^{-2}. As seen the capacitive current for electrodes aged up to 850 h of electrolysis is much higher than that of as prepared one. This refers to an increase in the electrochemical active surface of the electrode with electrolysis, probably due to the increase of Ir sites involved in the faradic process from the outer to the inner oxide layer and/or the oxidation of metallic Ir. Further increase in the electrolysis time leads to a reduction in the capacitive current of the polarized electrode. Finally, the electrode lost most of its capacitive charge after deactivation or failure. The results in Figs. 11 and 12 clearly indicate the formation and gradual growth of TiO_2 at the interface of $Sn_{1-x-y}Ir_xSb_yO_{2+0.5y}$/Ti electrodes with electrolysis.

4. DISCUSSION

The improvement in the $Sn_{1-x-y}Ir_xSb_yO_{2+0.5y}$/Ti electrode stability by the combination of Ir, Sn and Sb cations can be attributed to the formation of a solid solution of a single phase triple oxide with more even and dense structure than IrO_2.

In accordance with the previous results, it seems reasonable that the failure of $Sn_{1-x-y}Ir_xSb_yO_{2+0.5y}$/Ti triple oxide electrodes can be attributed to the formation and growth of the TiO_2 interlayer during electrolysis [24,25]. Because of the electrochemical stability and the even structure of the ternary oxide, the formation of TiO_2 interlayer at the interface of these electrodes during electrolysis is driven by both of O^{2-} ions migration and diffusion through the oxide structure. These processes seem to be controlled by Ir content, which affected both the electrical conductivity and grain size of the oxide structure [29]. In other words, the delay of Ti passivation by increasing Ir content in $Sn_{1-x-y}Ir_xSb_yO_{2+0.5y}$/Ti electrodes can be interpreted in terms of an increase in both the electrical conductivity and grain size of the oxide structure.

On the other hand, the life of $Mn_{0.92}Mo_{0.07}Sn_{0.01}O_{2.07}/Sn_{1-x-y}Ir_xSb_yO_{2+0.5}$/Ti anode must be dependent upon the physical unevenness and defects of the intermediate layer. The expected local growth of TiO_2 oxide bumps under the thinner parts and/ physical defects of the intermediate IrO_2 layer led to the local destruction of the outer electrocatalyst layer, exposing directly IrO_2 with a high activity for chlorine evolution to the NaCl solution. However, even if the intermediate layer is uniform and compact as in the case of $Sn_{1-x-y}Ir_xSb_yO_{2+0.5y}$ triple oxides, the inward diffusion of oxygen through the electrocatalyst and intermediate layers is inevitable, and even if the 100% oxygen evolution efficiency is maintained the electric resistance of these anodes will continue to increase due to uniform growth of titanium oxide.

5. CONCLUSIONS

$Sn_{1-x-y}Ir_xSb_yO_{2+0.5y}$ electrocatalysts coated-Ti substrate were examined as new intermediate layers of the anodes consisting of the outer γ-MnO_2 type MnMoSn-oxide electrocatalyst for oxygen evolution during seawater electrolysis at of 1000 Am^{-2} in 0.5 M NaCl solution of pH 8.7.

1. The performance of the anodes with the $Sn_{1-x-y}Ir_xSb_yO_{2+0.5}$ intermediate triple oxide layers, with sufficient Ir content, is superior to that of the anode with the intermediate IrO_2 layer.
2. The longest life was realized by the formation of uniform and compact intermediate $Sn_{1-x-y}Ir_xSb_yO_{2+0.5}$ triple oxide layer. Unevenness and high porosity of the intermediate IrO_2 layer was responsible for the shorter life.
3. The increase of the life of the anode with the increase in Ir content in the intermediate $Sn_{1-x-y}Ir_xSb_yO_{2+0.5}$ triple oxide layer was related to an increase in grain size and electrical conductivity of the oxide structure.

ACKNOWLEDGEMENTS
Dr. Ahmed Abd El-Moneim would like to express his sincere gratitude to Emeritus Professor Dr. Koji Hashimoto of Tohoku Institute of Technology, Sendai, Japan for providing the research facilities of coating, XRD measurements and an opportunity to visit Tohoku Institute of Technology, Japan as a Visiting Research Fellow supported by Daiki Atika Engineering Co. Ltd., Japan.

References

1. A.A. El-Moneim, N. Kumagai, K. Asami and K. Hashimoto, *Materials Trans.* 46(2005)309-316.
2. K. Izumiya, E. Akiyama, H. Habazaki, N. Kumagai, A. Kawashima, K. Hashimoto, *Electrochim. Acta* 43(1998) 3303–3321.
3. K. Fujimura, T. Matsui, K. Izumiya, N. Kumagai, E. Akiyama, H. Habazaki, A. Kawashima, K. Asami, K. Hashimoto, *Mater. Sci. Eng*. A267 (1999) 254–259.
4. K. Fujimura, T. Matsui, H. Habazaki, A. Kawashima, N. Kumagai, K. Hashimoto, *Electrochim. Acta* 45 (2000) 2297–2303.
5. A.A. El-Moneim, N. Kumagai and K. Hashimoto, *Materials Trans.* 66 (2009)1969 -1977.
6. A.A. El-Moneim, *Int. J. of Hydrogen Energy* 36 (2011) 13398-13406.
7. N.A. Abdel Ghany, N. Kumagai, S. Meguro, K. Asami, K. Hashimoto, *Electrochim. Acta* 48 (2002) 21–28.
8. N.A. Abdel Ghany, S. Meguro, N. Kumagai, K. Asami, K. Hashimoto, *Mater. Trans*. 44 (2003) 2114–2123.
9. A.A. El-Moneim, N. Kumagai, K. Asami, K. Hashimoto, *ECS Trans.* 1 (4) (2006) 491–497.
10. A.A. El-Moneim, J. Bhattarai, Z. Kato, K. Izumiya, N. Kumagai, K. Hashimoto, *ECS Trans*. 25 (40) (2010) 127–137.
11. W. Badawy, K. Doblhofer, I. Eiselt, H. Gerischer, S. Krause, J. Melsheimer, *Electrochim. Acta* 29 (1984) 1617-1623.
12. C. Iwakura and K. Sakamoto, *J. Electrochem. Soc*. 132 (1985) 2420-2423.
13. M. Ito, Y. Murakami, H. Kaji, K. Yahikozawa, Y. Takasu, *J. Electrochem. Soc.* 143(1)(1996) 32-36.
14. J. Gaudet, A.C. Tavares, S. Trasatti, D. Guay, *Chem. Mater*. 17 (2005)1570-1579.
15. A.I. Onuchukwu, S. Trasatti, *J. Appl. Electrochem.* 21 (1991) *858*-862.
16. J. Forti, P. Olivi, A.R. Andrade, *J. Electrochem. Soc.* 150 (4)(2003) E222-E226.
17. H-B Xu, Yong-Hong Lu, Chun-Hu Li and Jie-Zhen Hu, *J. Appl. Electrochem*. 40 (2010) 719-727.
18. E.N. Balko, P.H. Nguyen, *J. Appl. Electrochem*. 21 (1991) 678-682.
19. L. K. Xua and J. D. Scantlebury, *J. Electrochem. Soc.* 150 (6) (2003) B254-B261.
20. L.M. Da Silva, D.V. Franco, L.A. De Faria, J.F.C. Boodts, *Electrochimica Acta* 49 (2004)3977-3988.
21. C.P. De Pauli, S. Trasatti, *J. Electroanal. Chem*. 396 (1995) 161-168.
22. J. F. C. Boodts *and* S. Trasatti, *J. Electrochem Soc.* 137 (1990) 3784.
23. X. Chen and G.Chen, *Electrochimica Acta* 50 (20) (2005) 4155-4159.
24. X.M. Chen, G.H. Chen, P.L. Yue, *J. Phys. Chem*. B 105 (2001)4623-4628.
25. A.A. El-Moneim and H.M. Soliman, *Int. J. of Sustainable Water and Environmental Systems* 2(1) (2011) 43-48.
26. H. Habazaki, T. Matsui, A. Kawashima, K. Asami, N. Kumagai, K. Hashimoto, *Scr. Mater*. 44 (2001) 1659–1662.
27. H. Habazaki, T. Matsui, A. Kawashima, K. Asami, N. Kumagai, K. Hashimoto, *J. Appl. Electrochem.* 32 (2002) 993–1000.
28. P. Scherrer, *Gottingen Nachrichen*, 2 (1918) 98.

29. Z. Kato, J. Bhattarai, K. Izumiya, N. Kumagai, K. Hashimoto, *Appl. Surface Science*, 257(9)(2011)8230-8236.

© 2012 by ESG (www.electrochemsci.org)